Scanning frequency mixing microscopy of high-frequency transport behavior at electroactive interfaces

Brian J. Rodriguez and Stephen Jesse
Materials Science and Technology Division, Oak Ridge National Laboratory, Oak Ridge, Tennessee 37931

Vincent Meunier
Computer Science and Mathematics Division and Center for Nanophase Materials Sciences, Oak Ridge National Laboratory, Oak Ridge, Tennessee 37831

Sergei V. Kalinin[a)]
Materials Science and Technology Division, Oak Ridge National Laboratory, Oak Ridge, Tennessee 37931

(Received 23 November 2005; accepted 18 February 2006; published online 7 April 2006)

An approach for high-frequency transport imaging, referred to as scanning frequency mixing microscopy (SFMM), is developed. Application of two high-frequency bias signals across an electroactive interface results in a low-frequency component due to interface nonlinearity. The frequency of a mixed signal is chosen within the bandwidth of the optical detector and can be tuned to the cantilever resonances. The SFMM signal is comprised of an intrinsic device contribution and a capacitive mixing contribution, and an approach to distinguish the two is suggested. This technique is illustrated on a model metal-semiconductor interface. The imaging mechanism and surface-tip contrast transfer are discussed. SFMM allows scanning probe microscopy based transport measurements to be extended to higher, ultimately gigahertz, frequency regimes, providing information on voltage derivatives of interface resistance and capacitance, from which device characteristics such as Schottky barrier height, etc., can be estimated. © *2006 American Institute of Physics*. [DOI: 10.1063/1.2192977]

Progress in miniaturization of electronic components as well as rapidly emerging nanoscale sensors and electronic devices necessitate the development of techniques for assessing and imaging device operation on the nanometer scale. In the last decade, techniques such as scanning surface potential microscopy[1,2] (SSPM) and scanning impedance microscopy[3,4] (SIM) have been employed for quantitative dc (SSPM), ac (SIM), and nonlinear[5] (NL-SIM) transport imagings in semiconductor structures, metal-semiconductor interfaces, and grain boundaries. However, the frequency range accessible by these techniques is limited by the bandwidth of the optical detector in force-sensitive probe microscopies (~1–3 MHz). In addition, the signal is strongly dependent on the dynamic behavior of the cantilever. The high-frequency region in SPM can be accessed using mixed frequency techniques, based, with few exceptions,[6,7] on current detection.[8–12] Here, we develop an approach for high-frequency transport imaging, further referred to as scanning frequency mixing microscopy (SFMM), based on the force detection of a mixed frequency signal at nonlinear electroactive interfaces, and analyze the relevant image formation mechanism.

SFMM is implemented on a commercial SPM system (Veeco MultiMode NS-IIIA) equipped with external function generators and lock-in amplifiers (DS 345 and SRS 830, Stanford Research Instruments, Model 7280, Signal Recovery). The system is additionally equipped with an external data acquisition system developed in LABVIEW/MATLAB for bias and frequency spectroscopy of interfaces and emulation of multiple data acquisition channels. As a test for the technique, we used a prototypical metal-semiconductor interface prepared by cross sectioning a commercial Au–Si Schottky diode[4] (barrier height, ϕ_B=0.55 eV; saturation current, $I_0 = 7.83\times10^{-6}$ A; leakage resistance, 600 kΩ) connected in series with two current limiting resistors (R in the range of 1–33 kΩ), as illustrated in Fig. 1(a). Measurements were performed using Cr–Au coated tips (CSC-38 C, Micromasch, $l \approx 300$ μm, resonant frequency ~14 kHz) in the dual-pass mode with a typical lift height of 200 nm. A lock-in amplifier

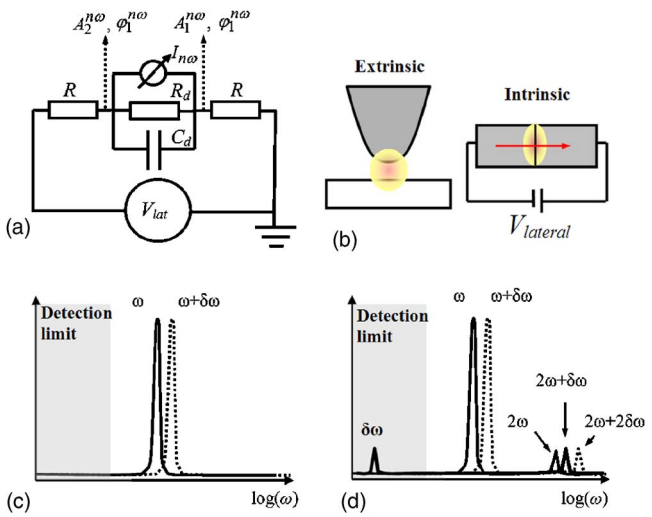

FIG. 1. (Color online) (a) Equivalent circuit in SFMM. (b) Extrinsic and intrinsic contributions to SFMM signals. (c) In a linear system, the application of a high-frequency probing signal generates potential oscillations only on the main harmonics of the signal. (d) In a nonlinear system, frequency mixing on the nonlinear element gives rise to potential oscillations on the main harmonics of the probing signal as well as second harmonics, sum signal, and difference signals.

[a)]Author to whom correspondence should be addressed; electronic mail: sergei2@ornl.gov

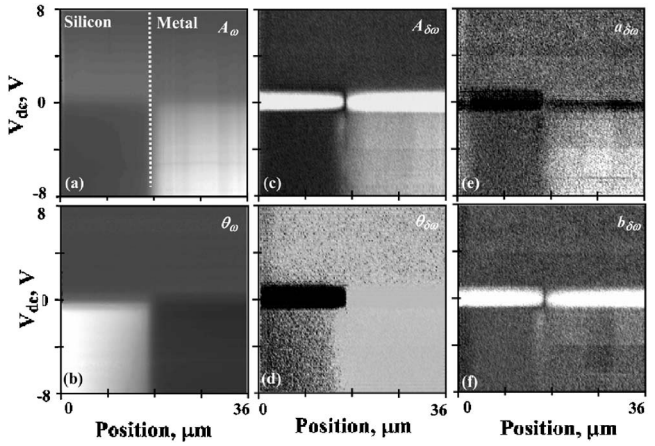

FIG. 2. (Color online) 2D maps of dc bias dependence of amplitude [(a) and (c)] and phase [(b) and (d)] of the first harmonic [(a) and (b)] and mixed frequency [(c) and (d)] signals. Position of the interface is indicated with a dotted line in (a). The strong feature at ~0 V in frequency mixing signal (c) is due to the intrinsic contribution. (e) Intrinsic and (f) extrinsic parts of the mixed frequency signal.

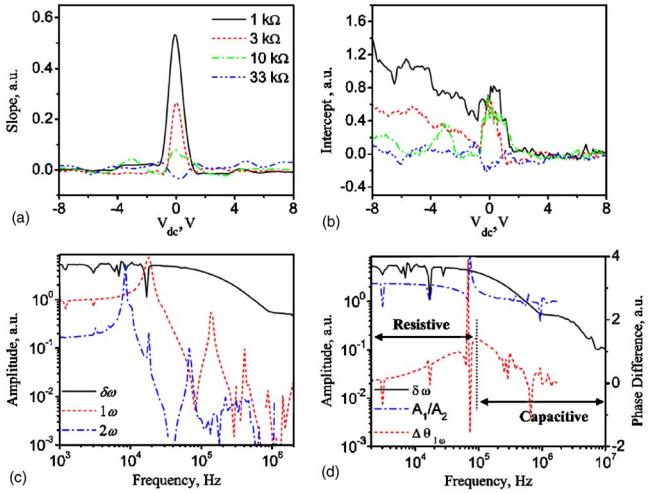

FIG. 3. (Color online) Bias dependence of intrinsic (a) and extrinsic (b) contributions to the mixed frequency signal. (c) Frequency dependence of the mixed frequency (solid) and first (dot) and second (dash dot) responses. (d) Frequency dependence of mixed frequency (solid), and phase difference (dash) and amplitude ratio (dash dot) of the first harmonic response.

is used to determine the magnitude and phase of the cantilever response at ω or $\delta\omega$. The output amplitude and phase shift signals are stored in an external control computer as a function of frequency, dc bias applied across the device, and position on device surface (slow scan axis disabled), producing two dimensional (2D) spectroscopic maps that illustrate frequency/bias, coordinate/bias, or coordinate/frequency dependences of response signal.

In SFMM, the modulation signal, $V_{\text{lat}}=V_{\text{dc}}+V_1\cos(\omega t)+V_2\cos[(\omega+\delta\omega)t]$, is applied across the experimental circuit as shown in Fig. 1(a), where ω is chosen in the 1 kHz–40 MHz range (limited by the function generator), and $\delta\omega$ is typically 10 kHz. Correspondingly, the surface potential has a dc component $V_{0\omega}(x)$ and components at the frequencies of lateral bias, $V_\omega(x)$ and $V_{\omega+\delta\omega}(x)$. The detailed analysis of the dc and first harmonic responses is reported elsewhere.[4,5] In nonlinear systems, frequency mixing at electroactive interfaces results in additional terms at higher-order and mixed harmonics of the modulation signal. Particularly of interest is the low-frequency component $V_{\delta\omega}\cos(\delta\omega t)$ that can be tuned to be within the bandwidth of optical detection for arbitrarily high ω.

The oscillating bias results in capacitive force acting on the dc biased tip,

$$2F_{\text{cap}}(z)=C_z'(V_{\text{tip}}-V_{\text{surf}})^2, \tag{1}$$

where V_{tip} is the tip bias, and C_z' is the tip-surface capacitance gradient, resulting in the transfer between the voltage oscillations of the surface and cantilever amplitude. However, this quadratic dependence of the tip-surface force also results in an additional frequency mixing between modulation signals. Thus, the SFMM signal is a sum of an intrinsic signal generated in the device, $F_{\delta\omega}^{\text{int}}$, and an extrinsic signal generated in the tip-surface junction, $F_{\delta\omega}^{j}$:

$$F_{\delta\omega}=F_{\delta\omega}^{\text{int}}+F_{\delta\omega}^{j}\sim V_{\delta\omega}(V_{\text{tip}}-V_{0\omega})+V_1V_2. \tag{2}$$

Notice that the intrinsic term is linear in tip bias, while the extrinsic term is tip bias independent. Hence, the intrinsic contribution can be selected by acquisition of data at several (e.g., 3) different tip biases and detecting the slope of local response-bias curve, or by using an additional lock-in and periodically varying the tip bias V_{tip} to determine the linear component.

Similarly to linear and nonlinear SIMs, the amplitude of the tip vibration is proportional to the corresponding harmonic of the bias, while the phase is shifted by a position-independent term. Thus, measuring the phase and amplitude of the tip oscillation allows the phase and amplitude of the surface voltage oscillations to be mapped.

Device mapping using SFMM is illustrated in Fig. 2. The spatial distribution of the first harmonic amplitude and phase signal (SIM) as a function of lateral bias is illustrated in Figs. 2(a) and 2(b). As previously reported,[4,5] the amplitude and phase shifts develop across the interface under reverse bias conditions, while under forward bias, there is only a small signal variation due to the work function difference between metal and semiconductor. The maps of amplitude and frequency of the mixed signal (SFMM) are shown in Figs. 2(c) and 2(d). Note that the amplitude variation is step-like for large reverse biases, exactly zero for forward biases, and contains a sharp feature at the zero bias, i.e., in the region of maximum nonlinearity of the *I-V* curve. This agrees with the predictions of Eq. (2), where at large negative biases, the extrinsic contribution dominates, while at zero bias, the intrinsic term dominates.

To distinguish and separate these contributions, we have acquired the response maps for several tip biases and numerically determined the slope and intercept of the corresponding best linear fit at each point in the (V_{lat},x) phase space. The resulting slope and intercept maps are shown in Figs. 2(e) and 2(f), providing the decomposition of intrinsic and extrinsic signals. This behavior is further elucidated in Figs. 3(a) and 3(b) where we examine the line profiles along the voltage axis. Note that the extrinsic signal is independent of the surface work function, a feature that constitutes a clear advantage compared to standard SIM. The linear component can also be selected using a second lock-in amplifier and by periodically modulating tip bias.

To analyze SFMM dynamics, the responses at ω (SIM), 2ω and 3ω (NL-SIM), and $\delta\omega$ (SFMM) were measured simultaneously as a function of frequency (ω varied, $\delta\omega$

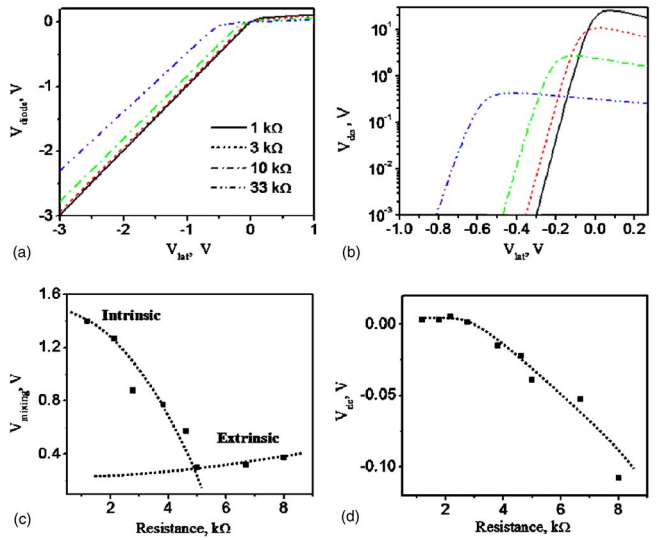

FIG. 4. (Color online) (a) Theoretical voltage characteristics and (b) mixed frequency response of the Schottky diode calculated using Eq. (3). (c) Experimental maximum amplitude of SFMM signal for different circuit terminations. The crossover from an intrinsic to an extrinsic signal is observed. (d) Bias corresponding to the SFMM maximum. Dotted line emphasizes the trend.

=10 kHz), as shown in Fig. 3(c). From this data, it is apparent that the present approach provides an effective method to decouple the dynamic behavior of the system and the detector. While harmonic signals show strong frequency dependence as expected for a cantilever, the SFMM signal is virtually independent on the carrier frequency. Finally, Fig. 3(d) compares SIM and SFMM signals. The regions of resistive and capacitive coupling across the interface are clearly seen in the phase signal. Note that the SFMM signal is virtually frequency independent below the crossover frequency and decays above it due to reduced interface impedance. Moreover, the SFMM signal can be measured well above the SIM limit, opening the potential for high-frequency measurements of active devices.

To relate the SFMM mechanism to device properties, we expand the *I-V* curve of the interface in a Taylor series as $I(V_0+\delta V)=I_0+(\partial I/\partial V)\delta V+0.5(\partial^2 I/\partial V^2)\delta V^2+o(\delta V^3)$, where the derivatives of the *I-V* curve are calculated around the dc bias V_0 across the interface. For the diode interface, this expansion is valid for a potential drop across the diode $\tilde{V}_0 < 27$ mV to ensure convergence. The nonlinear element behaves as a current source at $\delta\omega$, connected in parallel with nonlinear interface resistance and grounded through circuit termination resistances [Fig. 1(a)]. The amplitudes of the SFMM signal can be derived as

$$V_{\text{mixing}} = \frac{V_1 V_2 R}{4}\frac{\partial^2 I}{\partial V^2}\left[\frac{R(\tilde{V}_0)}{2R+R(\tilde{V}_0)}\right]^3, \tag{3}$$

where $\tilde{V}_0 = V_{\text{lat}}\{R(V_{0\omega})/[R(V_{0\omega})+2R]\}$.

For a symmetric circuit, the amplitudes of the intrinsic SFMM signals are equal on both sides of the interface, whereas, the phase changes by 180°, in agreement with the experimental observations.

While Eq. (3) is difficult to apply analytically, we can compare the model and experimental results by estimating numerically the response of the experimental system using predetermined device parameters (saturation current and Schottky barrier height). The numerically calculated potential drop across the interface and SFMM signal as a function of circuit termination resistance and lateral bias are illustrated in Figs. 4(a) and 4(b). Note that SFMM signal decreases with the resistance *R*, and the signal maximum shifts to negative biases. Corresponding experimental behavior is shown in Figs. 4(c) and 4(d), in agreement with the model calculations.

To summarize, the nonlinear high-frequency transport behavior across electroactive interfaces can be accessed using a mixed frequency transport imaging technique, referred to here as SFMM. Both intrinsic frequency mixing in the device and electrostatic frequency mixing in the tip-surface junction contribute to the measured signal. These contributions can be separated using approaches based on a secondary tip bias modulation. Compared to SIM and NL-SIM signals, the SFMM signal has a much weaker frequency dependence, and therefore allows for the decoupling of material and probe dynamics. The extension of SPM-based transport measurements to the high-frequency regime will provide information on device behavior under conditions of operation, and allow *in situ* characterization of device operation on the nanoscale.

Two of the authors (S.V.K. and V.M.) acknowledge support from ORNL Laboratory Research and Development funding. Oak Ridge National Laboratory is managed by UT-Battelle, LLC, for the U.S. Department of Energy under Contract No. DE-AC05-00OR22725.

[1] A. Chavez-Pirson, O. Vatel, M. Tanimoto, H. Ando, H. Iwamura, and H. Kanbe, Appl. Phys. Lett. **67**, 3069 (1995).
[2] B. D. Huey and D. A. Bonnell, Appl. Phys. Lett. **76**, 1012 (2000).
[3] S. V. Kalinin and D. A. Bonnell, Appl. Phys. Lett. **78**, 1306 (2001).
[4] S. V. Kalinin and D. A. Bonnell, J. Appl. Phys. **91**, 832 (2002).
[5] J. Shin, V. Meunier, A. P. Baddorf, and S. V. Kalinin, Appl. Phys. Lett. **85**, 4240 (2004).
[6] Z. Weng, C. J. Falkingham, G. E. Bridges, and D. J. Thomson, J. Vac. Sci. Technol. **20**, 999 (2002).
[7] B. T. Rosner and D. T. van der Weide, Rev. Sci. Instrum. **73**, 2505 (2002).
[8] S. J. Stranick and P. S. Weiss, Rev. Sci. Instrum. **64**, 1232 (1993).
[9] S. J. Stranick and P. S. Weiss, Rev. Sci. Instrum. **65**, 918 (1994).
[10] J.-P. Bourgoin, M. B. Johnson, and B. Michel, Appl. Phys. Lett. **65**, 2045 (1994).
[11] G. P. Kochanski, Phys. Rev. Lett. **62**, 2285 (1989).
[12] J. Schmidt, D. H. Rapoport, and H.-J. Frohlich, Rev. Sci. Instrum. **70**, 3377 (1999).